Molecular ordering and motion within the smectic-E phase: ^{2}H NMR study

Nuno A. Vaz,* Maria J. Vaz, and J. William Doane
Department of Physics and Liquid Crystal Institute, Kent State University, Kent, Ohio 44242
(Received 2 March 1984)

Unusual deuterium NMR spectral patterns are reported for a magneto-aligned, smectic-E sample consisting of a binary mixture of 4-n-butoxybenzylidene-4′-n-octylaniline-2,3,5,6-d_4 (4O.8-d_4) and 50 wt. % 4-n-octyloxycyanobiphenyl (8OCB). This spectral behavior is consistent with the para axis of the aromatic ring of 4O.8 being perfectly ordered ($S=0.99\pm0.01$) in the smectic-E phase. The short axis of the ring is also ordered, however, not perfectly ordered, on the average, and undergoing π flips about the para axis on a time scale $\lesssim 10^{-5}$ sec. There are found to be two possible motional models for the orientational ordering of the short axis of the ring that are consistent with the data: (1) molecular diffusion about the herringbone lattice with angular jumps of 44° between lattice sites, or (2) on-site librational motion with an in-plane order parameter of 0.80 for the degree of order of the short axis. Upon transforming from the smectic-B to the smectic-E phase in this material the degree of order of the para axis of the ring is observed to change continuously.

I. INTRODUCTION

The smectic-E, S_E, phase appears to be one of the most highly ordered varieties of liquid crystalline polymorphism. There are only a few examples of such phases reported to appear at temperatures below it prior to solidification.[1,2] Furthermore, several sharp x-ray Bragg reflections, some of which exhibit all three Miller indices different from zero, and a relatively small sized unit cell[3–7] suggest a relatively well defined and compact molecular packing.

Recent x-ray diffraction studies have shown that molecular positional and orientational correlations extend both in a direction perpendicular to the smectic layers and within the layers.[5–7] To describe the molecular packing within each layer one may represent the molecules as rods of elliptical cross section; such ellipses are then found to pack in a herringbone fashion as shown schematically in Fig. 1. By comparing the lattice parameters that can be calculated from x-ray diffraction patterns with the known molecular dimensions it is self-evident that the rotational freedom about the molecular long axis should be restricted.[5–8] Leadbetter *et al.*[9] have used incoherent quasielastic neutron scattering experimental techniques to conclude that the molecular motion within a S_E phase should consist primarily of (i) rapid ($t\sim 10^{-11}$ sec) localized diffusive motion (of 1 to 2 Å) perpendicular to the smectic layers, and (ii) overdamped librations ($\sim 30°$) about the molecular long axes. Only within a smectic-B (S_B), smectic-A (S_A), or a nematic (N) phase would the molecules be found to experience rotational freedom about their long molecular axes.

In this paper we report the first detailed deuterium NMR study of molecular orientational ordering in the S_E phase. This study is confined to the ordering of one aromatic ring segment of the molecule. The ^{2}H NMR technique is well suited for this study as it is highly sensitive to orientational ordering and the characteristic time scale of the measurement is $\gtrsim 10^{-5}$ sec, much larger than that of the typical neutron scattering experiment ($\sim 10^{-10}$ sec), allowing us to probe molecular motions over a much longer period of time.[10]

The results of this study are quite intriguing from an NMR point of view in that new spectral patterns are reported with unusual features. From a materials point of view new insight is gained on the ordering and motion of the aromatic ring in the S_E phase. One surprising feature is that the S_E phase has a molecular order parameter S for the long molecular axis near unity. The short axis of the aromatic ring is also well ordered but undergoes small amplitude librations and 180° flips about its para-axis direction on a time scale $\lesssim 10^{-5}$ sec.

II. EXPERIMENTAL RESULTS

The sample consisted of a binary mixture of 4-n-octyloxycyanobiphenyl (8OCB) and 4-n-butyloxybenzylidene-4′-n-octylaniline selectively deuterated in the ani-

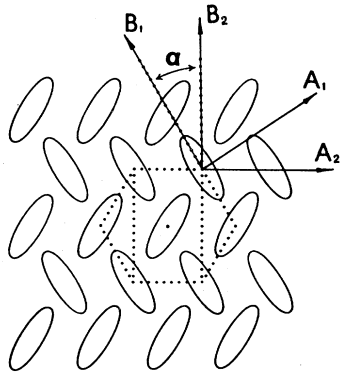

FIG. 1. Schematic representation of the in-plane molecular herringbone packing of the smectic-E phase illustrating the jump angle α and the time-averaged principal axes A_1, B_1, and C_1, and A_2, B_2, and C_2 used in the models described in the text. The C_1 and C_2 directions are normal to the page.

 ©1984 The American Physical Society

line aromatic ring (4O.8-d_4, see Fig. 2) at positions 2, 3, 5, and 6. While in pure form each of these materials exhibit the following polymorphism (respectively and with the temperatures in degrees centigrade): $C \rightarrow S_A$, 54°; $S_A \rightarrow N$, 67°; $N \rightarrow I$, 80°; and $C \rightarrow S_B$, 30°; $S_B \rightarrow S_A$, 48°; $S_A \rightarrow N$, 63°; $N \rightarrow I$, 79°. Their binary mixtures on the other hand are known[11] to exhibit the S_E phase. This is a feature that appears to have some generality in the sense that equimolar mixtures of 8OCB and several other nO.m Shiff base materials also exhibit a S_E phase. As such we prepared a mixture containing 50 wt.% of 4O.8-d_4 and 50 wt.% 8OCB for which the polymorphism as detected under the polarizing microscope is as follows: $C \rightarrow S_E$, 15°; $S_E \rightarrow S_B$, 52.9°; $S_B \rightarrow S_A$, 83°; $S_A \rightarrow S_A + I$, 104°; $S_A + I \rightarrow I$, 107.5°.

Deuterium NMR spectral patterns were recorded at 30.8668 MHz using a superconducting coil magnet (Narolac) and a home-built spectrometer. In order to reduce spectral distortions we used a modified quadrupole echo pulse sequence.[12] The delay between pulses was 100 μsec. The sample temperature was regulated via a controlled gas nitrogen flow to within ± 0.5 °C both in temperature stability and gradient; of more importance was a precise (< 0.1°) angular orientation of the sample with respect to the direction of the external applied magnetic field, which was achieved with a specially constructed NMR probehead.

Although the mesogenic mixture exhibited no nematic phase, the existence of a two-phase region of isotropic and S_A phases allowed for the preparation of a magneto-aligned sample in which the director could be uniformly aligned. The transition temperatures as determined from abrupt changes in the ^{2}H NMR spectral features were found to be $C \rightarrow S_E$, 15°; $S_E \rightarrow S_B$, 52.5°; $S_B \rightarrow S_A$, 83.2°; $S_A \rightarrow S_A + I$, 98.7°; $S_A + I \rightarrow I$, 107.5°; these values are in good agreement with those measured from observations under the polarizing microscope. The sample was first heated up into the isotropic phase and the data were then recorded in a slowly cooling cycle. Data were also recorded as a function of the orientation of the sample with respect to the direction of the applied magnetic field at several selected temperatures. As will be discussed later, some differences could be noticed in the spectral line shapes recorded within the S_E phase, if the data were recorded by first preheating the sample to the isotropic melt and then cooling it to a predetermined temperature before a new angular dependence of the spectral splitting was to be made.

Figure 3 shows an ^{2}H NMR spectrum consisting of one pair of lines (or doublet) from the deuterated aromatic ring with a frequency separation (or splitting $\delta\nu$) which is illustrative of all spectral patterns recorded within the S_A, S_B, and S_E phases for the case where the sample director (layer normal) is parallel to the direction of the applied magnetic field. The second doublet of reduced intensity which is observed at large frequencies in Fig. 3 is due to the spurious deuteration which took place during the selective deuteration process. It did not appear to disturb the interpretation of the results.

Figure 3 also shows the temperature dependence of the spectral splitting when the sample is oriented with its director (layer normal) parallel to the direction of the applied magnetic field. Most of the phase transitions are discernible on the temperature axis by the observed discontinuous jumps in the spectral splitting $\delta\nu$. Only the $S_B \rightarrow S_E$ phase transition appears somewhat masked. However, the angular dependence of the spectral line shape was observed to abruptly change at 52.5 °C, thus unambiguously identifying the position of this phase transition. Interestingly, while this phase transition appears masked in the ^{2}H NMR results of Fig. 3, it was quite easily detected under the polarizing microscope by the sudden appearance of cross striations on the focal-conic texture. In contrast, the S_A to S_B phase transition which is clearly revealed in the ^{2}H NMR data (Fig. 3), goes almost unperceived when observed under the polarizing microscope.

The spectral frequencies $\pm\nu$ were observed to change as the angle between the direction of the applied magnetic

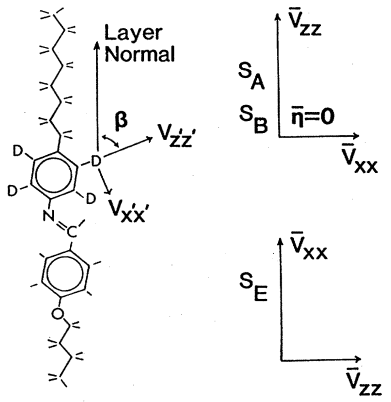

FIG. 2. Illustration of the molecular structure of 4O.8-d_4 and the principal axes (X',Y',Z') associated with the C—D bond where Y' is normal to the plane of the aromatic ring. Also illustrated are the time-averaged principal-axes directions X,Y,Z in the S_A, S_B, and S_E phases where Y is normal, on the average, to the plane of the ring.

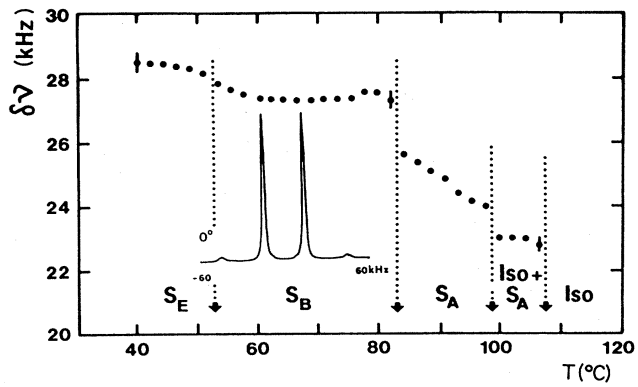

FIG. 3. Temperature dependence of the spectral splittings and an illustrative spectrum recorded from 4O.8-d_4 in a binary mixture with 50 wt.% 8OCB within the S_A, S_B, or S_E phases for the case where the sample director is parallel to the direction of the applied magnetic field.

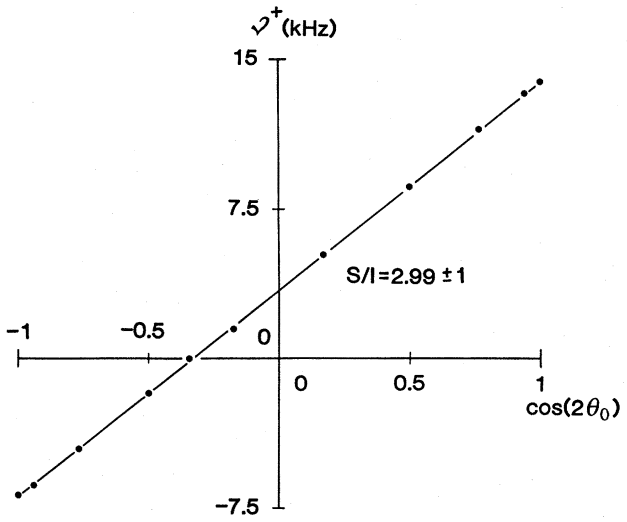

FIG. 4. Angular dependence of one of the spectral frequencies recorded within the S_B phases.

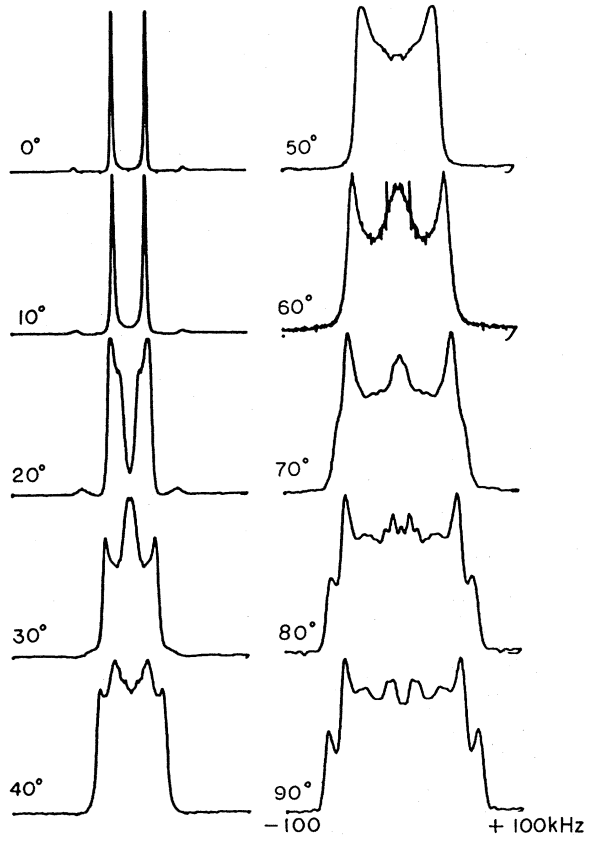

FIG. 5. Spectral patterns recorded at different angles of sample orientation in the magnetic field and at a temperature of 20 °C within the S_E phase. The spectral width of each of the patterns is 200 kHz.

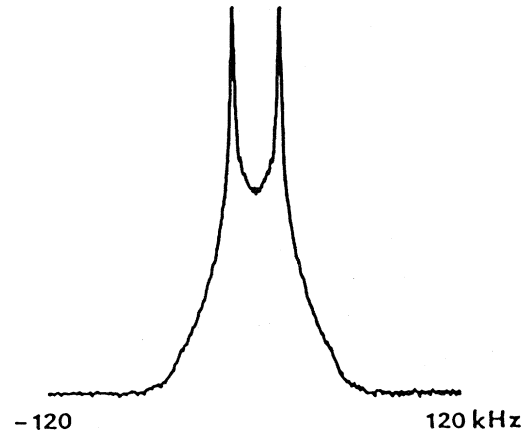

FIG. 6. Spectral pattern recorded in the S_E phase from a sample prepared by heating from the crystalline solid phase.

field and the sample orientation θ_0 was varied. Within the S_A and S_B phases, that angular dependence $\pm\nu(\theta_0)$ was found to be like that illustrated in Fig. 4. In this figure $\nu(\theta_0)$ is plotted versus $\cos(2\theta_0)$ to illustrate the expected uniaxial character of both the S_A and S_B phases (to be discussed in more detail later).

Within the S_E phase, however, the angular dependence of the spectral line shape was found to be totally different. Figure 5 illustrates the results obtained at selected angles. Notice that the spectral width for $\theta_0=90°$ is much larger than that at $\theta_0=0°$, which is in contrast with the results obtained within the S_A and S_B phases—compare with Fig. 4 at $\cos(2\theta_0)=-1$ and $+1$, respectively.

Finally, if the sample were heated from the solid to the S_E phase without ever reaching one of the higher temperature phases, the resulting spectral line shape is that illustrated in Fig. 6. If there were no alignment by the magnetic field this spectrum would correspond to a sample in which the director (layer normal) would be randomly distributed. Analysis indicates, however, partial alignment in certain regions of the sample by the magnetic field.

III. SPECTRAL ANALYSIS

The deuterium quadrupole interaction is observed as a perturbation on the Zeeman interaction. In the fast-motion regime, a spin $I=1$ gives rise to a spectrum of two lines with spectral frequencies given by[13]

$$\nu^{\pm}=\pm\tfrac{3}{16}\bar{\nu}_Q\{[1+\bar{\eta}\cos(2\phi_0)]+[3-\bar{\eta}\cos(2\phi_0)]\times\cos(2\theta_0)\}\,, \quad (1)$$

where θ_0 and ϕ_0 are the spherical coordinate angles giving the direction of the applied magnetic field in the frame of the principal-axis system of the electric-field-gradient tensor. The time-averaged coupling constant $\bar{\nu}_Q=(eQ/h)\bar{V}_{ZZ}$, where e is the electron charge, Q the quadrupole moment of the nucleus, h the Planck constant, and $\bar{V}_{ZZ}$ the largest component of the averaged field-gradient ten-

sor; the quantity $\bar{\eta}=(\bar{V}_{XX}-\bar{V}_{YY})/\bar{V}_{ZZ}$ is the motionally induced asymmetry parameter and is normalized to $0\leq\bar{\eta}\leq 1$ by choosing the labeling of the principal-axis frame (PAF) such that $|\bar{V}_{XX}|\leq|\bar{V}_{YY}|<|\bar{V}_{ZZ}|$.

The S_A and S_B phases are known to be uniaxial phases which implies that $\bar{\eta}=0$. This feature is confirmed in these materials by making a plot of $\nu^{\pm}$ versus $\cos(2\theta_0)$ which, from Eq. (1), should yield a straight line with a ratio between its slope S and its intercept of the ν^{+} axis I given by $S/I=[3-\bar{\eta}\cos(2\phi_0)]/[1+\bar{\eta}\cos(2\phi_0)]$. This ratio approaches the limit of 3 as $\bar{\eta}\rightarrow 0$ independent of the factor $\bar{\nu}_0$. The plot of Fig. 4 confirms that $\bar{\eta}=0\pm 0.003$ for the S_B phase and furthermore shows that in the preparation of the magneto-aligned phase the principal Z axis is aligned by the magnetic field to be parallel to $\vec{H}$. A similar feature was observed for the S_A phase. From these two features we know that fast molecular rotations, or at least rotations of the deuterated aromatic ring, are, on the average, unbiased and must take place, on the average, about an axis parallel to the layer normal.

One of the consequences of Eq. (1) is that for $\bar{\eta}=0$, $\nu(\theta_0=0°)=2|\nu(\theta_0=90°)|$. However, from Fig. 5 we see that such is not the case within the S_E phase where the spectral width increases rather than decreases with increasing values of θ_0. A significantly larger spectral width for $\theta_0=90°$ is an indication that, unlike the S_A and S_B phase, the largest component of the time-averaged electric-field-gradient tensor (Z component) is no longer parallel to the smectic layer normal. Furthermore, and in contrast with the S_A and S_B phases, the spectral lines evolve into spectral patterns (powder patterns) with edge singularities as the angle θ_0 is increased toward 90°.

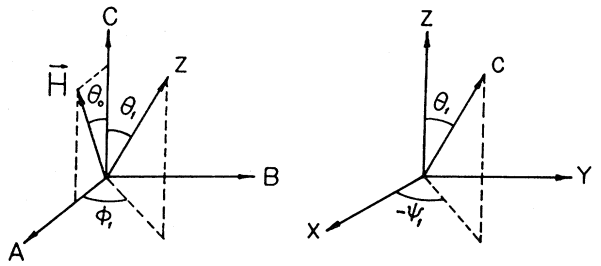

FIG. 7. Illustration of the reference frame and angles used in the text. The sample frame is that of A, B, C, where C is the axis aligned by the magnetic field upon cooling from the isotropic, through the S_A and S_B into the S_E phase. The principal-axis frame is that of (X,Y,Z).

This spectral behavior is easily explained by considering the time-averaged electric-field-gradient tensor to be substantially modified in the S_E phase such that the principal Z axis is no longer parallel to the bilayer normal (axis of magneto alignment) as in the S_A and S_B phases. In this regard it is convenient to introduce a frame fixed to the sample container (A,B,C), where the C axis is the axis of magnetic alignment achieved by cooling from the isotropic phase. Using the Euler angles (ϕ_1,θ_1,ψ_1) to express the orientation of the principal axis X,Y,Z frame in the A,B,C frame (see Fig. 7), we calculate

$$\begin{aligned}\nu^{\pm}=\pm\tfrac{3}{4}\bar{\nu}_Q\Big[&P_2(\cos\theta_0)\left[P_2(\cos\theta_1)+\frac{\bar{\eta}}{2}\sin^2\theta_1\cos(2\psi_1)\right]\\&+\tfrac{3}{4}\sin^2\theta_0\cos(2\phi_1)\left[\sin^2\theta_1+\frac{\bar{\eta}}{3}(1+\cos^2\theta_1)\cos(2\psi_1)\right]-\tfrac{3}{4}\sin^2\theta_0\sin(2\phi_1)\left[\frac{2\bar{\eta}}{3}\cos\theta_1\sin(2\psi_1)\right]\\&+\tfrac{3}{4}\sin(2\theta_0)\cos\phi_1\left[\sin(2\theta_1)-\frac{\bar{\eta}}{3}\sin(2\theta_1)\cos(2\psi_1)\right]+\frac{\bar{\eta}}{2}\sin(2\theta_0)\sin\phi_1\sin\theta_1\sin(2\psi_1)\Big]\,.\end{aligned}\tag{2}$$

In the S_A and S_B phases the Z axis is parallel to the C axis whereby $\theta_1=0$. Further assigning $\phi_1=\psi_1=0$, Eq. (2) reverts to Eq. (1). Upon passing into the S_E phase, however, the spectral behavior suggests that one of the other principal axes is parallel to C. If we assume this to be the X axis (to be justified later both theoretically and experimentally), then $\theta_1=90$ and $\psi_1=0$. If, in addition, we define $\omega^{\pm}=\nu^{\pm}/\frac{3}{8}\bar{\nu}_Q(\bar{\eta}-1)$, then Eq. (2) becomes

$$\omega^{\pm}=\pm[a+b\cos(2\phi_1)]\,,\tag{3}$$

where $a=P_2(\cos\theta_0)$ and $b=(\eta+3)\sin^2\theta_0/2(\eta-1)$. Since there is no preferential alignment of the (A,B) plane, ϕ_1 can be assumed to take on any value from zero to 2π with equal probability. From this we obtain a spectral distribution[14] $G(\omega^{\pm})d\omega^{\pm}=P(\phi_1)d\phi_1$. Since ϕ_1 is uniformly distributed in a plane $P(\phi_1)=$const in which case we calculate the spectral pattern $G(\omega)=G(\omega^{+})+G(\omega^{-})$ as

$$\begin{aligned}G(\omega)=G_0\{&[(\omega_1-\omega^{+})(-\omega_2+\omega^{+})]^{-1/2}\\&+[(\omega_1+\omega^{-})(-\omega_2-\omega^{-})]^{-1/2}\}\end{aligned}\tag{4}$$

and where $G_0=$const, $\omega_1=(a-b)$ and $\omega_2=(a+b)$; with $G(\omega^{+})$ defined with the limits $\omega_1<\omega^{+}<\omega_2$ and $G(\omega^{-})$ within the limits $-\omega_1<\omega^{-}<-\omega_2$. The frequencies ω_1 and ω_2 are not only limiting spectral frequencies but also from Eq. (4) are edge singularities and are clearly visible on the spectral patterns as seen in Fig. 5.

In Fig. 8 we show a plot of one half of the splitting between the edge singularities as a function of θ_0 normalized to its value at $\theta_0=0$. These curves are then fitted to the functions $\omega_1=a-b$ and $\omega_2=a+b$ with the only fitting

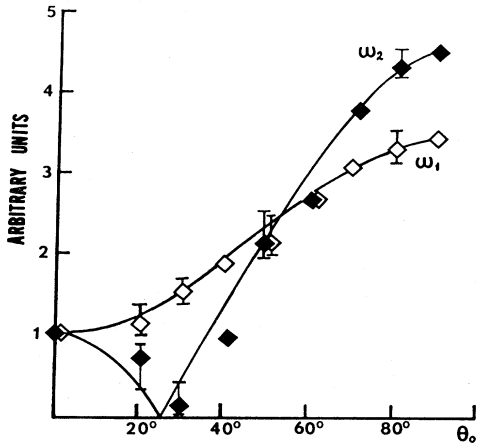

FIG. 8. Angular dependence of the splittings between the edge singularities normalized to their values at $\theta_0=0$. Solid lines are calculated curves with fitting parameters $\bar{\eta}=0.55\pm0.02$ and $\bar{\nu}_Q=86\pm3$ kHz.

parameter being the value of $\bar{\eta}$. The fits from Fig. 8 yield a value of $\bar{\eta}=0.55\pm0.02$ and from Eq. (3) a value of $\bar{\nu}_Q=86\pm3$ kHz. The fit to the points is reasonably good except near 20° where the fit is at the limits of the error. The reason for this deviation near small angles will be shown next to be due to the fact that θ_1 is not exactly 90°.

A more precise determination of $\bar{\eta}$ requires more precise spectral fits than Eq. (4) taking line broadening into account and examining more closely the assumption that $\theta_1=90°$. In order to do this we calculate the response function $g(t)$ calculated from[14]

$$g^{\pm}(t)=g_0\int_0^{2\pi}R(\sigma,t)\cos[2\pi\nu^{\pm}(\theta_0,\phi_1,\theta_1)t]d\phi_1\ , \qquad (5)$$

where $R(\sigma,t)$ is a distribution function of half-width σ that accounts for the intrinsic spectral line width. In principle R should also be a function of $\nu(\theta_0)$ but, in order to avoid cumbersome calculations, we simplified R to a simple Gaussian distribution function of fixed width. The Fourier transform of $g^{\pm}(t)$ gives $G^{\pm}(\nu)$ which is seen to be parametrized by $\bar{\nu}_Q$, $\bar{\eta}$, θ_1, and σ. Although five independent fitting parameters are to be adjusted, the final result is reliable in that each fitting parameter has a different characteristic effect on the spectral line shape. Furthermore, the range of values for each of them is quite restricted: $80\leq\bar{\nu}_Q\leq90$ kHz, $0.5\leq\bar{\eta}\leq0.7$, and $85°\leq\theta_1\leq90°$.

Figure 9 shows the calculated spectral patterns representing the best fits to the experimentally recorded patterns of Fig. 5. The best results (at this temperature of 20 °C) were obtained using the values $|\bar{\nu}_Q|=86.7$ kHz, $\bar{\eta}=0.57$, and $\theta_1=88.5\pm0.2°$. The general agreement is observed to be good except for the residual spectral intensity which is observed (at large angles) superimposed to the theoretically predicted line shape in the region of small frequencies. This is believed to be due to partial realignment of portions of the sample by the magnetic field. This residual component to the spectra became more pronounced at higher temperatures.

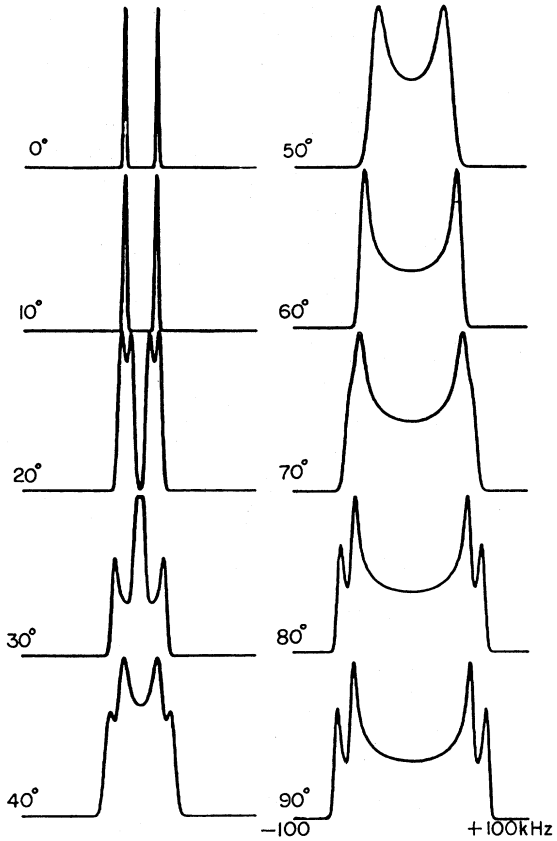

FIG. 9. Calculated spectral patterns that best fit the data shown in Fig. 5. The values of the fitting parameters are given in the text.

IV. MODELS FOR MOLECULAR MOTION

In this section we describe possible models to explain the measured values of $\bar{\eta}$ and $\bar{\nu}_Q$ for the S_A, S_B, and S_E phases. The electric-field-gradient tensor V at the nuclear site of a deuteron attached to a benzene ring at a sufficiently low temperature for which there is little molecular motion is characterized by having its largest principal component $V_{Z'Z'}$ along the C—D bond direction (Z' direction) and $\eta\simeq0.05$ with the X' axis on the plane of the ring.[15–17] The orientation of the PAF (X',Y',Z') at the deuteron nuclear site under this condition reflects the local symmetry of the atomic bondings. If motion is to occur on a time scale faster than the time scale of the ^{2}H NMR experiment ($\sim10^{-4}-10^{-5}$ sec) V will time average to some new values $\bar{V}$. The PAF of $\bar{V}$ should now further reflect the symmetries of the motion. If there are discrete orientations of the molecular segment, the resulting $\bar{V}$ can be calculated by taking the average

$$\bar{V}=\frac{1}{N}\sum_{i=1}^{N}P_iV^i\ , \qquad (6)$$

where V^i are the electric-field-gradient tensors for each ith orientation calculated on a common frame of reference. The time-averaged tensor is then calculated for N

orientations of the C—D bond direction. P_i are the corresponding probability densities of time occupancy. Once a model for the type of motion has been postulated, $\bar{V}$ can be calculated using Eq. (6) and then diagonalized. The orientation of the time-averaged PAF as well as values for $\bar{V}_{ZZ}$ and $\bar{\eta}$ can be determined and compared with experiment. The diagonalization procedure, however, can be avoided when the time-averaged PAF can be determined by symmetry. All that we usually may need is to specify the correspondence between the A_j,B_j,C_j frame ($j=1$ or 2 of Fig. 1) with the PAF (X,Y,Z) of $\bar{V}$ such as to ensure $|\bar{V}_{XX}| \leq |\bar{V}_{YY}| \leq |\bar{V}_{ZZ}|$ or, alternatively, that $0 \leq \bar{\eta} \leq 1$.

The tensors V at each of the N orientations of the C—D bond direction can be written in its PAF as

$$\underline{V} = V_{Z'Z'} \begin{bmatrix} -\frac{1}{2}(1-\eta) & 0 & 0 \\ 0 & -\frac{1}{2}(1+\eta) & 0 \\ 0 & 0 & 1 \end{bmatrix} \tag{7}$$

and, in the common frame reference, can be calculated using the rotation transformation[18] $V^i = R^{-1}(\phi_i',\theta_i',\psi_i')VR(\phi_i',\theta_i',\psi_i')$, where $R(\phi_i',\theta_i',\psi_1')$ is the rotation matrix[18] associated with the Euler angles $(\phi_i',\theta_i',\psi_i')$ that give the orientation of the C—D bond direction in that common frame of reference. The components of V^i are then given by

$$\begin{aligned}
V^i_{XX} &= \{(\tfrac{3}{2}\sin^2\theta_i'\cos^2\phi_i' - \tfrac{1}{2}) + \tfrac{1}{2}\eta[\cos(2\psi_i')(\cos^2\theta_i'\cos^2\phi_i' - \sin^2\phi_i') - \sin(2\psi_i')\sin(2\phi_i')\cos\theta_i']\}V_{Z'Z'} \\
V^i_{YY} &= \{(\tfrac{3}{2}\sin^2\theta_i'\sin^2\phi_i' - \tfrac{1}{2}) + \tfrac{1}{2}\eta[\cos(2\psi_i')(\cos^2\theta_i'\sin^2\phi_i' - \cos^2\phi_i') + \sin(2\psi_i')\sin(2\phi_i')\cos\theta_i']\}V_{Z'Z'} \\
V^i_{ZZ} &= \{(\tfrac{3}{2}\cos^2\theta_i' - \tfrac{1}{2}) + \tfrac{1}{2}\eta[\cos(2\psi_i')\sin^2\theta_i']\}V_{Z'Z'} \\
V^i_{XY} &= \{(\tfrac{3}{2}\sin^2\theta_i'\sin\phi_i'\cos\phi_i') + \tfrac{1}{2}\eta[\tfrac{1}{2}\cos(2\psi_i')\sin(2\phi_i')(\cos^2\theta_i' + 1) + \sin(2\psi_i')\cos(2\phi_i')\cos\theta_i']\}V_{Z'Z'} \\
V^i_{XZ} &= \{(\tfrac{3}{2}\sin\theta_i'\cos\theta_i'\cos\phi_i') + \tfrac{1}{2}\eta[-\tfrac{1}{2}\cos(2\psi_i')\cos\phi_i'\sin(2\theta_i') + \sin(2\psi_i')\sin\phi_i'\sin\theta_i']\}V_{Z'Z'} \\
V^i_{YZ} &= \{(\tfrac{3}{2}\sin\theta_i'\cos\theta_i'\sin\phi_i') + \tfrac{1}{2}\eta[-\tfrac{1}{2}\cos(2\psi_i')\sin\phi_i'\sin(2\theta_i') - \sin(2\psi_i')\cos\phi_i'\sin\theta_i']\}V_{Z'Z'} .
\end{aligned} \tag{8}$$

We will consider for simplicity that P_i is unity. Different models for the molecular motion can now be assumed.

A. S_A and S_B phases

A simple but useful model is one where the para axis of a benzene ring (1-4 direction) is an n-fold rotation axis. If $n \geq 3$ then Eqs. (6) and (8) yield $\bar{V}_{XX} = \bar{V}_{YY} = -\frac{1}{2}\bar{V}_{ZZ}$ and hence $\bar{\eta}=0$, the observed value in the S_A and S_B phases. In this model $\bar{\nu}_Q = \nu_Q[1-\frac{1}{2}(3-\eta)\sin^2\theta']$ where in the case of the benzene ring $\theta_1=\beta\simeq 60$, $\eta=0.05$, and $\nu_Q \simeq 182$ kHz yields a value of $|\bar{\nu}_Q| = 19.3$ kHz. In the S_A and S_B phases this value is further reduced by $\sim |\bar{\nu}_Q| S$, where S is the degree of order of the molecule. The experimental value of the coupling constant from Fig. 3 is $2\delta\nu/3 = 18.3$ kHz, yielding $S=0.95$ for the S_B phase.

B. S_E phase

From the simple geometry of a herringbone lattice we consider four basic types of motion for the benzene ring within the S_E phase.

Type 1: On-site "π-flips" where the 1-4 ring direction is a twofold rotation axis.

Type 2: Self-diffusion of the molecule about the herringbone lattice which provides "α jumps" as indicated in Fig. 1.

Type 3: The combined motion of types 1 and 2.

Type 4: On-site librations of the short axis of its aromatic ring.

1. *Motion of type 1*

For rapid π flips of the aromatic ring about its para axis, the time-averaged PAF will, by symmetry, be parallel to the axes A_1, B_1, and C_1 of Fig. 1. The correspondence between axes of the time-averaged PAF (X,Y,Z) and the directions A_1, B_1, and C_1 depend upon the angle β between the C—D bond direction and the para axis and the imposed condition $|V_{XX}| < |V_{YY}| < |V_{ZZ}|$. Allowing the aromatic ring to make π flips about the C_1 axis, relative to the A_1, B_1, C_1 frame, we calculate values for $\bar{\eta}$ (see Appendix) as indicated in Fig. 10 which indicates a value of $\bar{\eta}=0.67$ at $\beta=60°$ and $\eta=0.05$. This value is

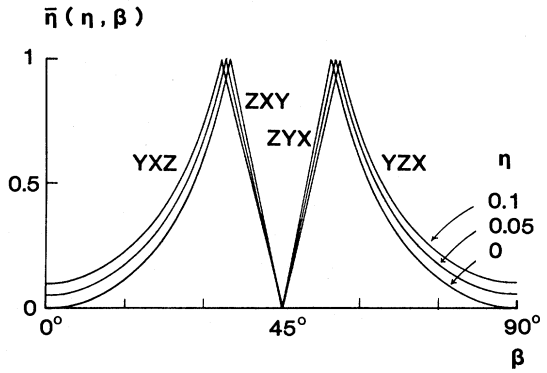

FIG. 10. Calculated time-averaged asymmetry parameter $\bar{\eta}$ from the π-flip (type 1) motional model of the deuterated benzene ring plotted as a function of the angle β between the C—D bond orientation and the para axis. The parameter η is the intrinsic asymmetry parameter (see text) and the principal axes X, Y, and Z are indicated corresponding to the directions A_1, B_1, and C_1, respectively, of Fig. 1 for each region of the plot.

larger than that measured ($\bar{\eta}=0.57$) although the X-principal axis is parallel to the C_1 axis and thereby layer normal, also an observed feature of the experiment. It is to be noted that a finite value for the intrinsic asymmetry parameter η increases the value of $\bar{\eta}$ shifting it further from its measured value. However, it is normally expected that $\eta \simeq 0.05$ for deuterium spins on aromatic sites.

From this model (see Appendix) we also calculate $\bar{\nu}_Q=(eQ\bar{V}_{ZZ}/h)=\nu_Q[(\frac{3}{2}\sin^2\beta-\frac{1}{2})+\frac{1}{2}\eta\cos^2\beta]=114.9$ kHz, where, as before, we have taken $\nu_Q=182$ kHz, $\beta=60°$, and $\eta=0.05$. The π-flip model values of this quantity are also larger than the measured values ($|\bar{\nu}_Q|=86.7$ kHz). We shall show subsequently that better agreement can be obtained with experiment by a modification of this model in one of two ways: by molecular diffusion about the herringbone lattice (type-3 motion) or by on-site librations of the short axis of the aromatic ring (motion of type 4).

Of better agreement with experiment is the value of $eQ\bar{V}_{XX}/h$ calculated from the π-flip model. From Eqs. (8) we calculate $(eQ\bar{V}_{XX}/h)=\nu_Q[(\frac{3}{2}\cos^2\beta-\frac{1}{2})+\frac{1}{2}\eta\sin^2\beta]$. Choosing $\beta=60$, $\eta=0.05$, and $\nu_Q=182$ kHz, we obtain $|\bar{\nu}_Q|=19.3$ kHz. This is compared with $\frac{2}{3}\delta\nu$ of Fig. 3 which also yields a value of 19.0 ± 0.2 kHz.

The π-flip model therefore indicates that the para axis of the ring is nearly perfectly ordered. If we write $eQ/h\,|\,\bar{V}_{XX}\,|_{\text{meas}}\simeq eQ/h\,|\,\bar{V}_{XX}\,|_{\text{calc}}S$, where S is the degree of order of the para axis relative to the layer normal, then we obtain $S=0.99\pm0.01$.

2. Motion of type 2

In this motion we consider the aromatic ring to undergo discrete changes in orientation between α and $-\alpha$ (see Fig. 1) as the molecule jumps by self-diffusion from site to site. For values of $0<\alpha<90°$ and for $\beta=60°$ it is seen by symmetry that such a motion by itself would not yield any axis of the time-average PAF to be parallel to the layer normal. Since the X axis of the time-averaged PAF is observed by experiment to be along the layer normal, we rule out this type of motion.

3. Motion of type 3

Here we combine the two preceding models to consider both π flips and α jumps. In this model we consider an exchange of the orientation of the aromatic between four possible and equally probable sites. Relative to the A_2,B_2,C_2 frame of Fig. 1 we consider the orientation of the Y' axis of the aromatic ring to exchange between α, $\alpha+\pi$, $-\alpha$, and $-\alpha+\pi$. The calculated results of this model (see Appendix) for $\bar{\eta}$ is shown in Fig. 11 for $\beta=60°$.

In order to agree with experiment we must choose the regions of α where X is parallel to the C_2 axis. From Fig. 11, this corresponds to the regions $0<\alpha\lesssim 30°$ and $50°\lesssim\alpha\leq 90°$. Since an analysis of both regions yield identical results we only show the results of the region $0<\alpha\lesssim 30°$ whereby, from the Appendix we calculate $\bar{\nu}_Q=\nu_Q[(5+\eta)-(9+5\eta)\sin^2\alpha]$ and $\bar{\eta}=[(3+7\eta)-(9+5\eta)\sin^2\alpha]/[(5+\eta)-(9+5\eta)\sin^2\alpha]$. If this model

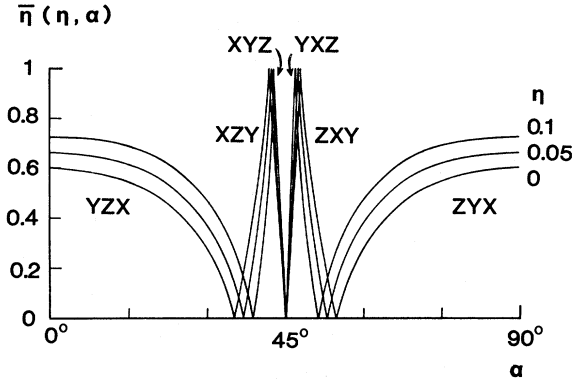

FIG. 11. Time-averaged asymmetry parameter $\bar{\eta}$ for the model involving the combined motion of π flip and α jumps of the deuterated benzene ring motion of type 3 plotted as a function of the angle α that measures the half amplitude of the jumps. The parameter η is the intrinsic asymmetry parameter (see text) and the time-averaged principal axes X, Y, and Z indicated are to be identified with A_2, B_2, and C_2, respectively, of Fig. 2.

is correct, then both the values of $\bar{\nu}_Q$ and $\bar{\eta}$ should agree with experiment (86.7 kHz and 0.57, respectively) for the given intrinsic values of ν_Q and η and a particular value of α. We find that this is indeed possible if we choose $\nu_Q=182$ kHz, $\eta=0.06$, and $\alpha=22°$. These values of η and ν_Q are well within their experimental uncertainty.[15–17] As noted above, the complementary value of $\alpha=78°$ will also provide agreement with experiment, but molecular packing models for this large angle appear somewhat unphysical.

It is interesting to note that this motional model also yields the result that the para axis of the ring is perfectly ordered. This follows from comparing $eq\bar{V}_{XX}/h$ with its experimental value. Equations (6) and (8) for this case yield $eq\bar{V}_{XX}/h=-\nu_Q(1-3\eta)/8=19.3$ kHz which, when compared to the value of 19.0 ± 0.2 kHz from Fig. 3, implies perfect order of the X' axis of the ring within experimental error.

4. Motion of type 4

Finally we consider a model of on-site librational motion of the short axis of the aromatic ring superimposed upon the π-flip model of type 1. In this model we consider the values of $\bar{\eta}$ and $\bar{\nu}_Q$ of type-1 motion to become further time averaged to values of $\bar{\bar{\eta}}$ and $\bar{\bar{\nu}}_Q$ by librational motion of the Z and Y principal axis about a laboratory fixed axis $\bar{Z}$ (director) in the $\bar{Z},\bar{Y}$ plane as illustrated in Fig. 12. Defining $S_i=\langle\frac{3}{2}\cos^2\theta_i-\frac{1}{2}\rangle$ where the θ_i are defined in Fig. 12, we can write $S_X=-0.5$ as the π-flip model yields perfect order of the para axis of the ring. Using $S_X+S_Y+S_Z=0$ this averaging process gives

$$\bar{\bar{\nu}}_Q=\bar{\nu}_Q\left[S_Z\left[1+\frac{\bar{\eta}}{3}\right]-\frac{\bar{\eta}}{3}\right] \tag{9a}$$

and

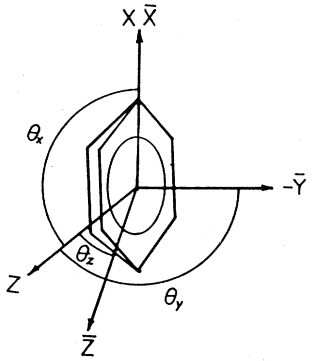

FIG. 12. Illustration of the principal axes X, Y, and Z associated with the aromatic ring following π flips about the X axis. The $\bar{X},\bar{Y},\bar{Z}$ frame is the principal-axis frame following librational motion of Z and Y about X.

$$\bar{\bar{\eta}}=\bar{\nu}_Q\left[S_Z\left[1+\frac{\bar{\eta}}{3}\right]-\left[1-\frac{2\bar{\eta}}{3}\right]\right]\Big/\bar{\bar{\nu}}_Q\,, \tag{9b}$$

where S_Z is the degree of order of the short molecular axis in the plane of the layer. Using the values of $\bar{\nu}_Q$ and $\bar{\eta}$ from the π-flip model (114.9 kHz and 0.67, respectively), Eqs. (9a) and (9b) both yield the result of $S_Z=0.8$ when the experimental values of 86.7 kHz and 0.67 are used for $\bar{\bar{\nu}}_Q$ and $\bar{\eta}$, respectively.

V. DISCUSSION

All of the motional models and the experimental data yield the result that the degree of order of para axis of the aromatic ring S relative to the axis of magneto alignment (layer normal) in the S_E phase is near perfect with $S=0.99\pm0.01$. Furthermore, the observed orientation of the time-averaged principal axis of the field-gradient tensor indicates that the ring is undergoing π flips about its para axis. Two different possible models, however, are able to account precisely for the measured values of the time-averaged coupling constant and asymmetry parameter: (1) molecular diffusion about a herringbone lattice with a herringbone structural angle of $\alpha=22°\pm0.5°$, (2) on-site librational motions of the short axis of the aromatic ring with an order parameter of $S_Z=0.8$. The former result depends on the value of the diffusion constant D and the time scale of the measurement $\tau\sim10^{-5}$ sec. With a lattice parameter $d\sim5$ Å, the value of D must be $\gtrsim X^2/2\tau\sim10^{-10}$ cm^2/sec for the molecular diffusional model to hold. Since the value of D has been measured to be $\sim10^{-8}$ cm^2/sec in the S_B and S_E phases,[19,20] it does not appear unreasonable for the diffusional model to be the correct one. The measured angle of $\alpha=22°$ is also a reasonable value for this angle. As pointed out in the text, the complementary angle of 78° is also a model solution which gives the measured values of the time-averaged quadrupole parameter. This angle, however, does not conform well to space-filling models based on the lattice parameters measured by x-rays.[7,21]

From published data[22] on the S_E phase from other deuterated sites it is suggestive that only the aromatic ring may be flipping and that other segments of the molecule may be rotating more freely. This observation comes from angular-dependent spectral patterns of 4O.8-d_{21} (perdeuterated alkyl chain) mixed with 8OCB (50 wt. %)[22] which narrow at $\theta_0=90°$ rather than broaden, as in this study. More data, however, on fewer deuterated sites is needed to confirm this.

It would also be interesting to measure the order of the short molecular axis (or measured value of α) as a function of temperature approaching the S_E-S_B transition. In fact, from Fig. 3 this transition appears to set on continuously and shows a large pretransition effect. As described in the text, values of $\delta\nu$ of Fig. 3 are directly proportional to the degree of order of the para axis of the aromatic ring which appears to go continuously from a value of $S=0.94$ in the S_B phase to a value of $S=0.99$ in the S_E phase. It would be interesting to follow the order of the short axis of the ring in this same temperature region.

It is of interest to the NMR worker to examine the values of the intrinsic quadrupole interaction associated with the C—D bond on the aromatic ring as these values are not known to high precision in the current literature. As described in the text a choice of 182 kHz for the value of ν_Q forced us to use a value of $\eta=0.06\pm0.005$ to obtain consistency in our models. This might be viewed as giving a more precise value of η, however, this should be accepted only with caution as modeling is involved and there also is an uncertainty in ν_Q.

Another one of the unknowns in the problem is the exact geometry of the aniline (benzene) ring. Although expected to be nearly hexagonal, we tested for a possible departure from the hexagonal shape. Both a deviation towards an oblate or a prolate ring are admissible since only minor variations ($\sim1°$) on the angle β (see Fig. 10) are required to make appreciable changes in the model calculations—sufficient to offset, for example, the implications of $\eta=0.06$. In any case, such deviations could not be found to bring any better agreement with the experimental observations.

The unusual spectral patterns of Fig. 5 that we have reported and explained may be characteristic of other phases with the herringbone structure. Nearly a decade ago a similar spectral pattern for the $\theta_0=90$ orientation was reported, although left unexplained, by Deloche *et al.*[23] for the herringbone structure of the smectic-*VI* (currently reported as smectic-*H*) phase of TBBA.

Finally, we conclude that further NMR studies on other deuterated segments as well as more detailed studies (temperature dependencies) on the deuterated aromatic ring would bring a more complete understanding of the S_E phase and the S_B-S_E phase transition which from Fig. 3 appears continuous.

ACKNOWLEDGMENTS

The authors are indebted to Dr. Mary E. Neubert for the preparation of the materials used in this work and to Mr. Bao-Gang Wu for assisting them in recording some of the data. This work was supported in part by the Na-

tional Science Foundation under Solid State Chemistry Program Grant No. DMR-82-44468 and in part by an Exxon Education Foundation grant.

APPENDIX

The time averaged values of $\bar{V}_{ZZ}$ and $\bar{\eta}=\bar{V}_{XX}-\bar{V}_{YY}/\bar{V}_{ZZ}$ are calculated from Eqs. (6) and (8) for the various types of motions indicated in the text.

1. Motion of type 1

Considering the orientation of the C—D bond to be described by the Euler angles (ϕ',θ',ψ') in the A_1,B_1,C_1 frame of Fig. 1, π flips can be described by an exchange between the equally probable two orientations $(90,\theta',\psi')$ and $(-90,\theta',\psi')$. From Fig. 2, $\theta'=\beta$ and $\psi'=0$ since C_1 is in the $X'Z'$ plane. From Eqs. (6) and (8) under the condition $|V_{XX}|<|V_{YY}|<|V_{ZZ}|$ there are four possible choices for the orientation of X,Y,Z.

(a) $A_1,B_1,C_1=(Y,X,Z)$, where for $0\leq\sin^2\beta\leq(1-\eta)/(3-\eta)$,

$$\bar{V}_{ZZ}=[(\tfrac{3}{2}\cos^2\beta-\tfrac{1}{2})+\tfrac{1}{2}\eta\sin^2\beta]V_{Z'Z'}\ ,$$

$$\bar{\eta}=[3\sin^2\beta+\eta(2-\sin^2\beta)]/(2-3\sin^2\beta+\eta\sin^2\beta)\ .$$

(b) $(A_2,B_2,C_2)=(X,Z,Y)$, where for $(3+7\eta)/(9+5\eta)\leq\sin^2\alpha\leq4(1+\eta)/(9+5\eta)$, if $\eta\geq\frac{1}{2}$, $\bar{V}_{ZZ}$ is the same as above, $\bar{\eta}$ has the opposite sign from above.

(c) $(A_2,B_2,C_2)=(X,Y,Z)$, where for $4(1+\eta)/(9+5\eta)\leq\sin^2\alpha\leq\frac{1}{2}$,

$$\bar{V}_{ZZ}=-\tfrac{1}{2}(1+\eta)V_{Z'Z'}\ ,$$

$$\bar{\eta}=[(6\cos^2\beta-3)+\eta(1-2\cos^2\beta)]/(1+\eta)\ .$$

(d) $(A_1,B_1,C_1)=(-Z,Y,X)$, where for $\frac{1}{2}<\sin^2\beta<2(3-\eta)$ the solution is similar to case (c) with $\bar{\eta}\rightarrow-\bar{\eta}$.

2. Motion of type 3

Considering the orientation of the C—D bond to be described by the Euler angles (ϕ',θ',ψ') in the A_2,B_2,C_2 frame of Fig. 1, this model can be represented by an exchange between the equally probable orientations $(90°-\alpha,60°,0°)$, $(90°+\alpha,60°,0°)$, $(-90°-\alpha,60°,0°)$ and $(-90°+\alpha,60°,0°)$. From Eqs. (6) and (8), under the condition $|V_{XX}|<|V_{YY}|<|V_{ZZ}|$, there are six possible choices for the orientations of X,Y,Z.

(a) $(A_2,B_2,C_2)=(Y,Z,X)$, where for $0\leq\sin^2\alpha\leq(3+7\eta)/(9+5\eta)$ and $0\leq\eta\leq1/3$,

$$\bar{V}_{ZZ}=\tfrac{1}{8}[5+\eta-(9+5\eta)\sin^2\alpha]V_{Z'Z'}\ ,$$

$$\bar{\eta}=[(3+7\eta)-(9+5\eta)\sin^2\alpha]/[(5+\eta)+(9+5\eta)\sin^2\alpha]\ .$$

(b) $(A_2,B_2,C_2)=(X,Z,Y)$, where for $(3+7\eta)/(9+5\eta)\leq\sin^2\alpha\leq4(1+\eta)/(9+5\eta)$, if $\eta\geq\frac{1}{2}$, $\bar{V}_{ZZ}$ is the same as above, $\bar{\eta}$ has the opposite sign from above.

(c) $(A_2,B_2,C_2)=(X,Y,Z)$, where for $4(1+\eta)/(9+5\eta)\leq\sin^2\alpha\leq\frac{1}{2}$,

$$\bar{V}_{ZZ}=[(1-3\eta)/8]V_{Z'Z'}\ ,$$

$$\bar{\eta}=(9+5\eta)(1-2\sin^2\alpha)/(1-3\eta)\ .$$

For $\frac{1}{2}\leq\sin^2\alpha\leq1$ there are again three domains of solution each corresponding to one of the above, domains whereby $\sin^2\alpha$ is everywhere replaced by $\cos^2\alpha$. The PAF labeling is, respectively, for the cases corresponding to (a), (b), and (c) above, and (Z,Y,X), (Z,X,Y), and (Y,X,Z).

*Present address: General Motors Research Laboratory, Warren, MI 48090.

[1]H. Kresse and B. Gajewsha, Phys. Status Solidi A **64**, K161 (1981).

[2]N. A. P. Vaz, Z. Yaniv, and J. W. Doane, Mol. Cryst. Liq. Cryst. **101**, 47 (1983).

[3]S. Diele, P. Brand, and H. Sackmann, Mol. Cryst. Liq. Cryst. **17**, 163 (1972).

[4]D. Coates, K. J. Harrison, and G. W. Gray, Mol. Cryst. Liq. Cryst. **22**, 99 (1973).

[5]J. Doucet, A. M. Levelut, M. Lambert, L. Leibert, and L. Strzelecki, J. Phys. (Paris) Colloq. **36**, C1-13 (1975).

[6]A. de Vries, in *Liquid Crystals*, edited by F. D. Saeva (Dekker, New York, 1979), pp. 1—71.

[7]A. J. Leadbetter, J. Frost, J. P. Gaughan, and M. A. Mazid, J. Phys. (Paris) Colloq. **40**, C3-185 (1979); A. J. Leadbetter, M. A. Mazid, and K. M. A. Malik, Mol. Cryst. Liq. Cryst. **61**, 39 (1980).

[8]N. A. P. Vaz, Z. Yaniv, and J. W. Doane, Mol. Cryst. Liq. Cryst. **101**, 47 (1983).

[9]A. J. Leadbetter, R. M. Richardson, and J. C. Frost, J. Phys. (Paris) Colloq. **40**, C3-125 (1979).

[10]J. W. Doane, in *Magnetic Resonance of Phase Transitions*, edited by F. J. Owens, C. P. Poole, and H. A. Farach (Academic, New York, 1979), pp. 171—246.

[11]P. E. Cladis, Mol. Cryst. Liq. Cryst. **67**, 177 (1981).

[12]I. Solomon, Phys. Rev. **110**, 61 (1958); J. H. Davis, K. R. Jeffrey, M. Bloom, M. I. Valic, and T. P. Higgs, Chem. Phys. Lett. **42**, 390 (1976).

[13]M. H. Cohen and F. Reif, in *Solid State Physics*, edited by F. Seitz and D. Turnbull (Academic, New York, 1957), Vol. 5, pp. 321—438.

[14]A. Abragam, *The Principles of Nuclear Magnetism* (Oxford University, London, 1962), Chap. VII.

[15]J. C. Rowell, W. D. Phillips, L. R. Melby, and M. Panar, J. Chem. Phys. **43**, 3442 (1965).

[16]H. H. Mantsch, H. Hazimi, and I. C. P. Smith, in *Progress in NMR Spectroscopy*, edited by J. W. Emsley *et al.* (Pergamon, New York, 1977), Vol. 11, pp. 211—271.

[17]D. M. Ellis and J. L. Bhorkstam, J. Chem. Phys. **46**, 4460 (1967).

[18]M. E. Rose, *Elementary Theory of Angular Momentum* (Wiley, New York, 1957), Chap. IV.

[19]G. J. Kruger, Phys. Reports **82**, 231 (1982).

[20]R. M. Richardson, A. J. Leadbetter, C. J. Carlile, and W. S. Howells, Mol. Phys. **35**, 1697 (1978).

[21]A. de Vries, Mol. Cryst. Liq. Cryst. **63**, 215 (1981).

[22]R. Y. Dong, H. Schmiedel, N. A. P. Vaz, Z. Yaniv, M. E. Neubert, and J. W. Doane, Mol. Cryst. Liq. Cryst. **98**, 411 (1983).

[23]B. Deloche, J. Charvolin, L. Leibert, and L. Strzelecki, J. Phys. (Paris) Colloq. **36**, C1-21 (1975).